Quantitative Comparison of Analytic and Iterative Reconstruction Methods in 2- and 3-Dimensional Dynamic Cardiac ^{18}F-FDG PET

Mark Lubberink, PhD[1]; Ronald Boellaard, PhD[1]; Arno P. van der Weerdt, MD[2]; Frans C. Visser, MD, PhD[2]; and Adriaan A. Lammertsma, PhD[1]

[1]Department of Nuclear Medicine and PET Research, VU University Medical Centre, Amsterdam, The Netherlands; and [2]Department of Cardiology, VU University Medical Centre, Amsterdam, The Netherlands

The aim of this work was to compare the quantitative accuracy of iteratively reconstructed cardiac ^{18}F-FDG PET with that of filtered backprojection for both 2-dimensional (2D) and 3-dimensional (3D) acquisitions and to establish an optimal procedure for imaging myocardial viability with ^{18}F-FDG PET. **Methods:** Eight patients underwent dynamic cardiac ^{18}F-FDG PET using an interleaved 2D/3D scan protocol, enabling comparison of 2D and 3D acquisitions within the same patient and study. A 10-min transmission scan was followed by a 10-min, 25-frame dynamic 3D scan and then by a series of 10 alternating 5-min 3D and 2D scans. Images were reconstructed with filtered backprojection (FBP) or attenuation-weighted ordered-subsets expectation maximization (OSEM), combined with Fourier rebinning (FORE) for 3D acquisitions, applying all usual corrections. Regions of interest (ROIs) were drawn in the myocardium, left ventricle, and ascending aorta, with the last 2 being used to define image-derived input functions (IDIFs). Patlak graphical analysis was used to compare net ^{18}F-FDG uptake in the myocardium, calculated from either 2D or 3D data, after reconstruction with FBP or OSEM. Either IDIFs or arterial sampling was used as the input function. The same analysis was performed on parametric images. **Results:** A good correlation ($r^2 > 0.99$) was found between net ^{18}F-FDG uptake values for a myocardium ROI determined using each acquisition and reconstruction method and blood-sampling input functions. A similar result was found for parametric images. The ascending aorta was the best choice for IDIF definition. **Conclusion:** Good correlation and no bias of net ^{18}F-FDG uptake in relation to that based on FBP images, combined with less image noise, make 3D acquisition with FORE plus attenuation-weighted OSEM reconstruction the preferred choice for cardiac ^{18}F-FDG PET studies.

Key Words: cardiac PET; ^{18}F-FDG; iterative reconstruction; quantification

J Nucl Med 2004; 45:2008–2015

The use of iterative reconstruction methods, such as ordered-subsets expectation maximization (OSEM), rather than filtered backprojection (FBP) has been investigated in several oncologic PET studies. Apart from assessing lesion detectability (*1–4*), some of these studies have also investigated the effects of iterative reconstruction on quantitative accuracy (*5–7*), not only in oncology but also in quantitative brain studies. In contrast, little is known about the use of iterative reconstruction in cardiac PET (*8*). The same is true for the comparison of PET studies with (2-dimensional [2D]) and without (3-dimensional [3D]) interplane septa. Removal of the interplane septa in 3D PET significantly increases not only sensitivity but also the detection of scattered radiation, random coincidences, and detector dead time—all of which require appropriate correction methods. The quantitative accuracy of 3D brain studies has been well documented, and the use of 3D PET in lesion detection in oncology has also been studied (*9–14*). The use of 3D PET for quantitative cardiac studies has been investigated less extensively (*15–17*), although the scatter correction method used on many clinical scanners (*18,19*) was developed with quantitative cardiac 3D imaging in mind. Furthermore, many commercially available PET or PET/CT systems are no longer equipped with septa and are thus capable only of 3D acquisitions.

Myocardial viability studies that use ^{18}F-FDG with the aim of quantifying glucose metabolism require the measurement of plasma radioactivity. Instead of arterial blood sampling, an image-derived input function (IDIF) can be defined using the radioactivity concentration in the left ventricle, left atrium, ascending aorta, or descending aorta (*20–25*). In a previous study, the ascending aorta was found to be the best choice for defining IDIFs (*24*), using 2D acquisitions and reconstruction by filtered backprojection.

The purpose of the present study was to assess the quantitative accuracy of both iterative reconstruction and 3D acquisition for cardiac PET studies. To this end, an interleaved 2D/3D scan protocol was used to enable comparison of 2D and 3D imaging within the same patient and study,

and data were reconstructed with both FBP and OSEM. In addition, both arterial blood sampling and IDIFs were used as plasma input curves.

MATERIALS AND METHODS

PET Scanner

All measurements were performed using an ECAT Exact HR+ scanner (CTI/Siemens). Standard settings for data compression (maximum ring difference, mash, and span) were used, together with standard corrections for normalization, random coincidences, and dead time (26,27). Data were corrected for attenuation using a 10-min windowed transmission scan acquired with 3 rotating ^{68}Ge/^{68}Ga rod sources. Scatter correction was performed using the methods included in the scanner software. This correction involves a stationary convolution subtraction method in 2D mode (28) and a simulation-based method in 3D mode (29). The scaling factor in the 3D scatter-correction algorithm was modified to ensure accurate cross-calibration of 2D and 3D acquisitions (30).

Image Reconstruction

The 3D data were converted to 2D sinograms using Fourier rebinning (FORE) (31), the standard procedure in the ECAT 7.2 software, which does not include full 3D reconstruction algorithms. Images were reconstructed using FBP or attenuation-weighted OSEM (32) (6 iterations, 16 subsets) as implemented in the ECAT 7.2 software, applying a Hanning filter of 5 mm in full width at half maximum to ensure resolution matching between reconstruction methods (5–7), resulting in a transverse image resolution of around 7 mm in the center of the FOV.

Patients and Scan Procedure

Eight patients (all male; mean age, 65 y; range, 56–76 y), admitted for assessment of myocardial viability, were included. After a 10-min transmission scan, approximately 370 MBq of ^{18}F-FDG dissolved in 5 mL of saline were administered as a bolus and a 10-min 3D dynamic emission scan was acquired: 6×5 s, 6×10 s, 3×20 s, 5×30 s, and 5×60 s. This dynamic scan was then followed by a series of ten 5-min scans alternating between 3D and 2D modes, separated by the time necessary to retract or insert the septa.

Blood Sampling

The radioactivity concentration of arterial blood was measured online during the course of the scan (33). At set times, additional discrete blood samples were collected and the arterial line was flushed to avoid clotting. The arterial blood curve was corrected for delay relative to the measured total trues counting rates, by matching times at which 50% of the peak counting rate was reached in the up-slopes of trues and blood curves. The whole-blood and plasma radioactivity concentrations of the discrete samples were measured in a well counter, cross-calibrated against the PET scanner. The plasma input function was then derived by multiplying the measured whole-blood curve with a linear fit to the plasma-to-blood ratios obtained from the discrete samples.

ROI Analysis

A region of interest (ROI) was drawn around the contour of the myocardium (6 image planes, total volume of approximately 40 cm^3) in transaxial images reconstructed using either FBP or OSEM and acquired in either 2D or 3D mode. ^{18}F-FDG influx rate constants (K_i) for the whole myocardium were calculated with graphical analysis according to the Patlak method (34), using only the last 5 frames in either 2D or 3D mode for determination of the Patlak slope. Plasma radioactivity concentration determined by arterial blood sampling was used as the input function. Because net ^{18}F-FDG uptake, described by K_i, is directly proportional to glucose metabolic rate by multiplication with the plasma glucose concentration divided by the lumped constant (35,36), the K_i results of the present study are valid for glucose metabolic rates as well.

Parametric Image Analysis

All images were resampled to 1-cm^3 voxels. K_i images were calculated using the Patlak method, again for each combination of acquisition and reconstruction methods and with blood-sampling data as input function. Scatterplots were generated, comparing measured K_i in all voxels within a $10 \times 10 \times 15$ cm box around the heart for the various combinations of acquisition and reconstruction methods. Correlation coefficients and slopes of linear regressions were calculated. The data were also analyzed by Bland–Altman plots (37), assessing the differences between voxel values for various combinations of reconstruction and acquisition methods.

IDIFs

ROIs were drawn in the left ventricle (diameter, 15 mm; length, 6 image planes) and ascending aorta (diameter, 13 mm; length, 6 image planes) for definition of IDIFs. The same ROIs were used for images obtained using all combinations of acquisition and reconstruction methods. For definition of the 3D IDIFs, all frames acquired in 3D mode were used. For the 2D IDIFs, the first 10 min were assumed to be equal to the 3D IDIFs, after which the 2D frames were added. These IDIFs were then interpolated to the same time points as used for the continuous sampling curves by linear interpolation, and the plasma radioactivity concentration was calculated using the same plasma-to-blood data as used to correct the sampling data. Mean values of the IDIFs in the last 5 frames in either 2D or 3D mode were calculated and compared with the mean value of the sampling plasma curve at the corresponding midpoint times. The same comparison (3D only) was made for the areas under the first 90 s of the IDIF and the blood-sampling plasma curve. Subsequently, the IDIFs were used as the input function for calculation of myocardial K_i.

RESULTS

ROI Analysis

Figure 1 shows scatterplots of K_i based on myocardium ROIs in images acquired in either 2D or 3D mode and reconstructed using FBP or OSEM. A clear linear correlation without bias exists between the K_i values for all methods, with the square of the Pearson correlation coefficient being at least 0.99 for all scatterplots.

Parametric Image Analysis

^{18}F-FDG K_i parametric images of a typical patient are shown in Figure 2. Figure 3 shows scatterplots for all combinations of reconstruction and acquisition methods for another patient. Table 1 summarizes the results, giving mean values of the scatterplot slopes and intercepts, the Pearson correlation coefficients, and the absolute differences between the results obtained using the different meth-
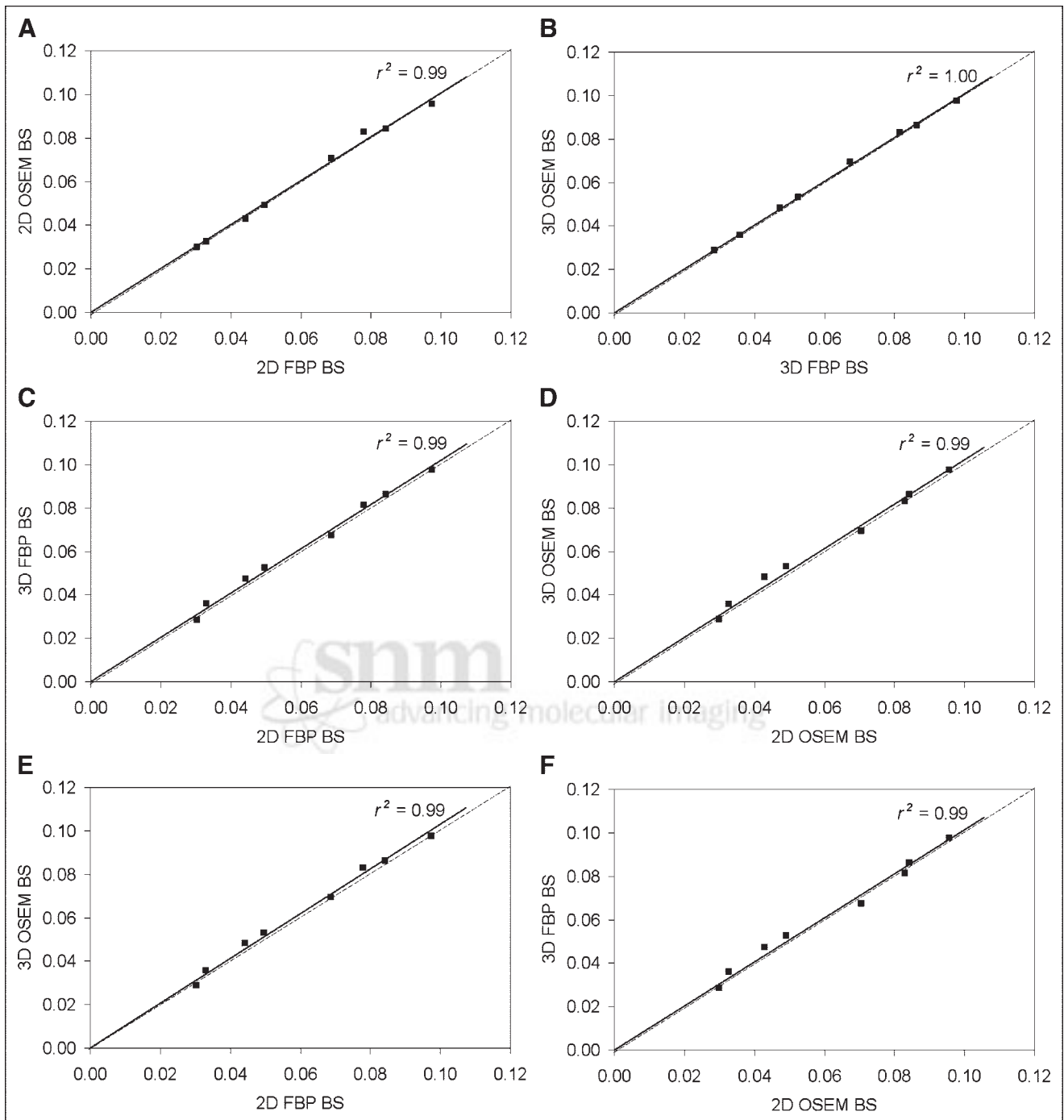
FIGURE 1. Scatterplots of myocardium K_i (min^{-1}) calculated using blood-sampling input function: 2D FBP vs. 2D OSEM (A), 3D FORE FBP vs. 3D FORE OSEM (B), 2D FBP vs. 3D FORE FBP (C), 2D OSEM vs. 3D FORE OSEM (D), 2D FBP vs. 3D FORE OSEM (E), and 2D OSEM vs. 3D FORE FBP (F). Each point represents K_i in myocardium ROI of one patient. Dotted lines are lines of identity, and solid lines are least-squares fits with zero intercept, for which squares of Pearson correlation coefficients are shown. BS = blood sampling.

ods. The results shown are for all voxels above a threshold at the mean of all voxel values within the image (a threshold chosen to include mainly voxels inside the myocardium).

IDIFs

The mean ratios of the IDIF relative to the blood-sampling curve during the last 10 frames and the area under the first 90s of the curve are given in Table 2. The area under the peak of the IDIF is significantly lower than the area under the peak of the blood-sampling curve, especially for images reconstructed by OSEM. The 2D IDIFs generally overestimate the input functions at later times, especially the left ventricle IDIFs. For images acquired in 3D mode, the
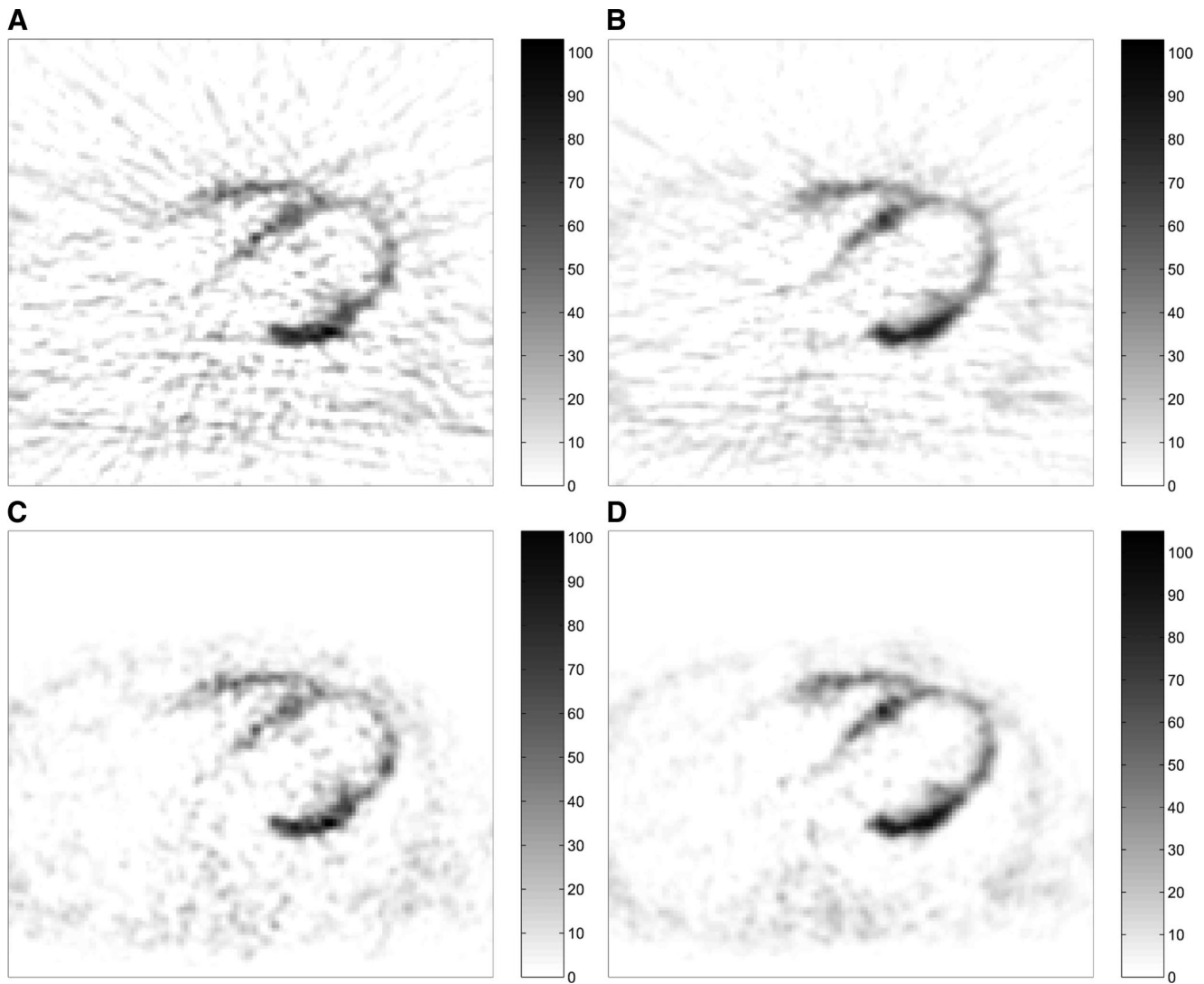
FIGURE 2. K_i (10^{-3} min^{-1}) parametric images of representative patient derived from 2D FBP (A), 3D FORE FBP (B), 2D OSEM (C), and 3D FORE OSEM (D) images and a plasma input function based on arterial sampling.

left ventricle IDIFs overestimate the input function whereas the ascending aorta IDIFs underestimate the input function.

Figure 4 shows scatterplots of K_i calculations based on IDIFs versus those based on blood-sampling input functions. With 8 data points and a significance of 0.05, an r^2 value below 0.45 is required to reject the hypothesis of a linear correlation with zero intercept, which is the case only for 2D FBP left ventricle IDIFs. Table 3 shows the ratios of K_i based on IDIFs and sampling data. Figure 4 and Table 3 clearly show that ascending aorta IDIFs resemble blood-sampling input functions better than do left ventricle IDIFs and that there is a larger spread in left ventricle data than in ascending aorta data. In addition, no significant differences were found between K_i values calculated using FBP and OSEM images with similar IDIFs and acquisition modes, and 3D images led to significantly higher K_i values than did 2D images with similar IDIFs.

DISCUSSION

Using an interleaved 2D/3D scanning protocol, the effects of both 2D and 3D acquisition protocols and analytic and iterative reconstruction techniques on quantitative cardiac ^{18}F-FDG PET studies were investigated. First, the effects of acquisition and reconstruction methods on K_i, calculated with blood-sampling data as the input function, were studied using either ROI or parametric analyses. Next, the quantitative effects of using an IDIF were assessed.

Good correlations were observed between K_i obtained from various combinations of acquisition and reconstruction methods, using continuous blood sampling as the input function and using either ROI analysis or parametric analysis. Neither 3D acquisition nor OSEM reconstruction led to a bias in K_i. No significant quantitative differences between cardiac studies reconstructed with OSEM and FBP and acquired in 2D or 3D mode were found.
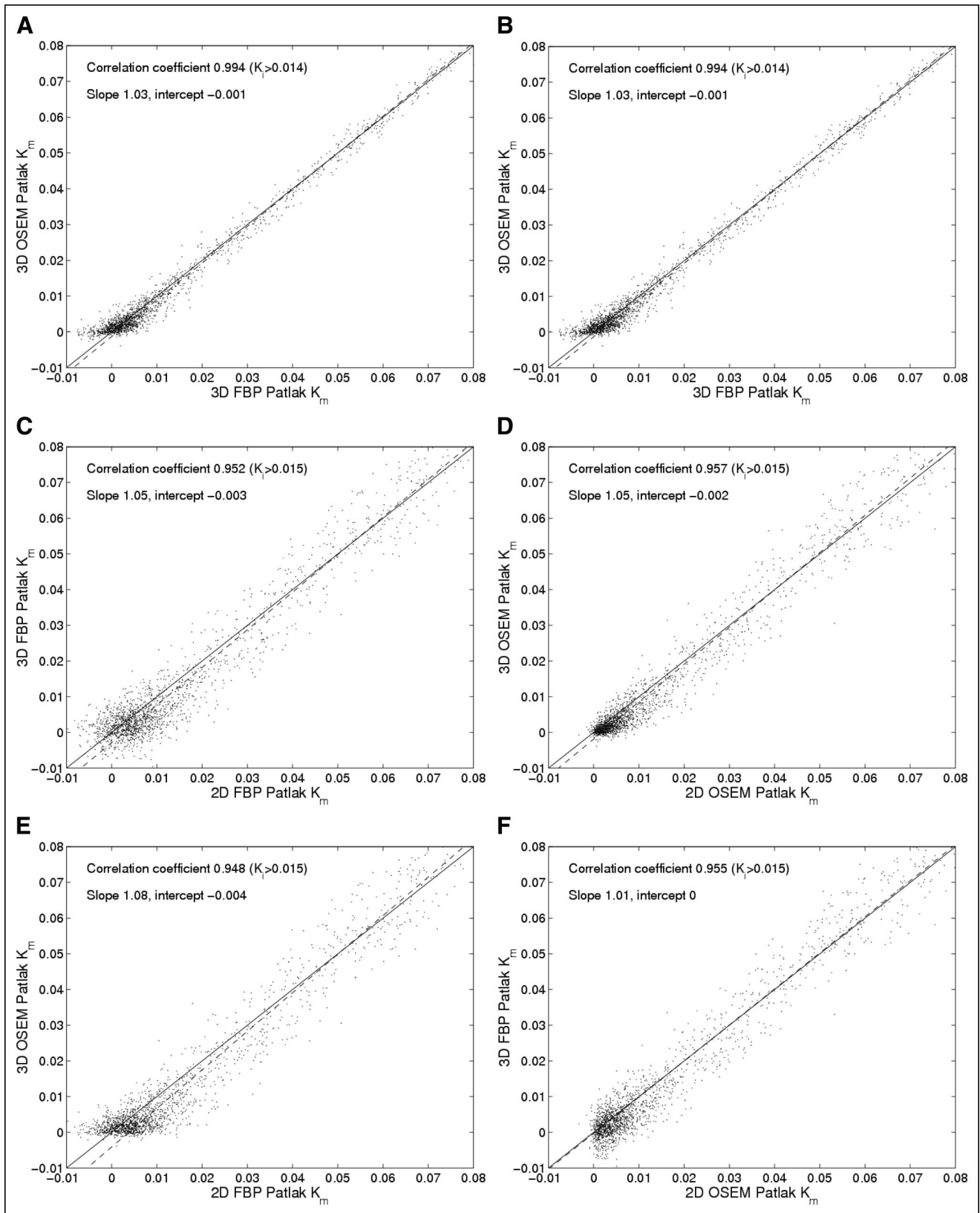
FIGURE 3. Scatterplots of K_i (min^{-1}) parametric images of representative patient: 2D FBP vs. 2D OSEM (A), 3D FORE FBP vs. 3D FORE OSEM (B), 2D FBP vs. 3D FORE FBP (C), 2D OSEM vs. 3D FORE OSEM (D), 2D FBP vs. 3D FORE OSEM (E), and 2D OSEM vs. 3D FORE FBP (F). Each point represents data from a 1-cm^3 cubic voxel. Solid lines in scatterplots are lines of identity; dashed lines are least-squares fits to all voxels in myocardium. $K_m = K_i$.

TABLE 1
Data from Scatter and Bland–Altman Analysis of Parametric Images

Parameter	2D FBP and 2D OSEM	2D FBP and 3D FBP	2D OSEM and 3D OSEM	3D FBP and 3D OSEM	2D FBP and 3D OSEM	2D OSEM and 3D FBP
Slope (K_i > threshold)	1.01 (0.02)	1.00 (0.06)	1.01 (0.05)	1.02 (0.01)	1.02 (0.06)	0.98 (0.05)
Intercept (K_i > threshold)	−0.001 (0.001)	−0.000 (0.002)	0.000 (0.001)	−0.001 (0.001)	−0.002 (0.002)	0.002 (0.001)
Correlation (r^2; all K_i)	0.99 (0.00)	0.97 (0.01)	0.98 (0.01)	0.99 (0.00)	0.97 (0.01)	0.98 (0.01)
Correlation (r^2; K_i > threshold)	1.000 (0.001)	0.991 (0.004)	0.992 (0.004)	0.999 (0.001)	0.990 (0.004)	0.992 (0.004)
Difference (K_i > threshold)	−0.0010 (0.0005)	−0.0003 (0.0011)	0.0007 (0.0011)	−0.0006 (0.0007)	−0.0004 (0.0012)	0.0013 (0.0013)

Data are mean and, in parentheses, SD. Threshold was chosen individually for each patient to include mainly voxels in myocardium.

3D IDIFs underestimate the blood radioactivity concentration during the first 90 s after administration, with a larger underestimation for images reconstructed by OSEM. During the late part of the input curve, all IDIFs except those using the ascending aorta in a 3D image overestimate the input function, with the 2D values being significantly higher than the corresponding 3D values. This overestimation is largest for 2D left ventricle IDIFs, and FBP and OSEM did not significantly differ in this case. The apparent overestimation of left ventricle IDIFs is likely caused by spillover of radioactivity from the myocardium. Because this effect is the same in 2D and 3D modes, the difference in overestimation between 2D and 3D left ventricle IDIFs may be caused by the different scatter-correction methods. Underestimation of the 3D ascending aorta IDIFs and the early part of the left ventricle IDIFs may be caused by the limited resolution of the scanner, resulting in a recovery of 80%–90% for a structure the size of the ascending aorta (*38*). In addition, the dead-time correction of the scanner may be inaccurate for a situation in which a large amount of radioactivity is concentrated in a small volume, such as the left ventricle and ascending aorta during the start of this scan, and especially in 3D acquisition mode because of the higher

counting rates. The underestimation in the early part of left ventricle IDIFs, as well as the overestimation during the late part of left ventricle IDIFs and better agreement between ascending aorta IDIFs and online input function, was also seen for 2D FBP images in an earlier publication (*24*).

The ratios between K_i for the whole myocardium calculated using ascending aorta IDIFs and blood sampling in 2D mode are consistent with those previously published (*24*), leading to the conclusion that the ascending aorta is the preferred choice for IDIF definition in 2D mode. This also seems to be the case in 3D mode, in which ascending aorta IDIFs lead to a minor overestimation and left ventricle IDIFs lead to a significant underestimation of K_i, compared with the blood-sampling input function.

Partial-volume correction of the ascending aorta IDIFs may be possible, but knowledge of the exact shape and size of the ascending aorta is needed for accurate correction. In the late part of the plasma curve, mainly determining the slope of the Patlak plot, the limited recovery in the myocardium may cancel out the limited recovery in the ascending aorta and thus not influence the Patlak slope. Partial-volume correction of the IDIF may lead to a smaller Patlak slope, but this effect is probably small. The limited recovery could also be improved by using less smoothing in OSEM reconstructions of 3D scans, possible because of the better statistics of 3D data. It should be noted that the 2D IDIFs contained a peak measured in 3D mode, which, as for the late part of the IDIFs, might have been higher had it been acquired in 2D mode. This higher peak, in turn, would have led to slightly smaller Patlak slopes for the 2D IDIFs. The linear correlation shown in Figure 4 leads to the conclusion that ascending aorta IDIFs can be used for Patlak analysis of cardiac ^{18}F-FDG scans without further partial-volume correction of the ascending aorta data.

The use of IDIFs enables modeling and quantitative analysis of tracer uptake without the need for arterial blood sampling. Earlier studies showed that the ascending aorta is the preferred choice for IDIF definition in 2D mode (*24*). This result was confirmed by the current study. K_i values

TABLE 2
IDIF vs. Blood Sampling

Method	Late IDIF/sampler	Peak IDIF/sampler
FBP, 2D, LV	1.60 (0.52)	
FBP, 3D, LV	1.19 (0.32)	0.81 (0.16)
FBP, 2D, AA	1.13 (0.10)	
FBP, 3D, AA	0.91 (0.09)	0.84 (0.17)
OSEM, 2D, LV	1.53 (0.43)	
OSEM, 3D, LV	1.20 (0.29)	0.78 (0.16)
OSEM, 2D, AA	1.17 (0.13)	
OSEM, 3D, AA	0.92 (0.10)	0.75 (0.14)

LV = left ventricle; AA = ascending aorta.
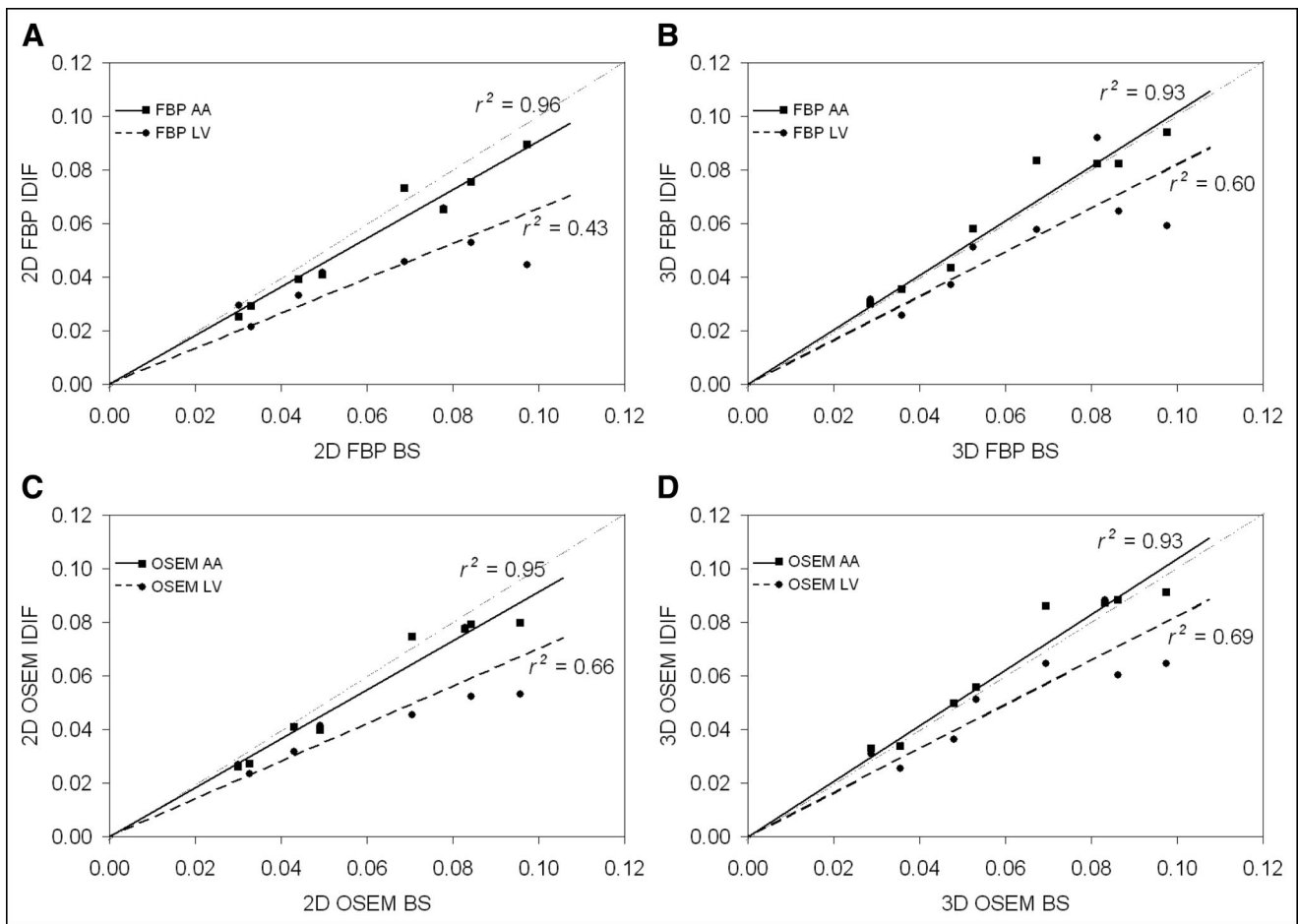Data are mean and, in parentheses, SD.

FIGURE 4. Scatterplots of myocardium K_i (min^{-1}) calculated using blood-sampling input function or IDIF: 2D FBP (A), 3D FORE FBP (B), 2D OSEM (C), and 3D FORE OSEM (D). Each point represents K_i in myocardium ROI of 1 patient. Dotted lines are lines of identity, and solid (ascending aorta [AA] IDIF) and dashed (left ventricle [LV] IDIF) lines are least-squares fits with zero intercept, for which squares of Pearson correlation coefficients are shown. BS = blood sampling.

based on IDIFs were significantly higher for 3D acquisitions than for 2D acquisitions. Further investigations—of, for example, the effect of the different scatter-correction algorithms in 2D and 3D PET studies—are required. Ascending aorta IDIFs are preferred to left ventricle IDIFs because they have a smaller deviation from the online plasma input function and are more reproducible, as shown by the lower SDs in Table 3. For nonlinear analysis using compartmental modeling, continuous blood sampling probably remains the

TABLE 3
Ratio of IDIF K_i to Sampling K_i

Method	FBP	OSEM
2D, LV	0.77 (0.18)	0.79 (0.15)
3D, LV	0.87 (0.19)	0.86 (0.17)
2D, AA	0.92 (0.11)	0.92 (0.10)
3D, AA	1.03 (0.10)	1.05 (0.10)

LV = left ventricle; AA = ascending aorta.
Data are mean and, in parentheses, SD.

method of choice, but for Patlak linear analysis of cardiac ^{18}F-FDG PET scans, ascending aorta IDIFs may be a sufficiently accurate alternative.

The use of 3D acquisition results in higher-quality images with the same amount of radioactivity because of the increase in scanner sensitivity. Alternatively, compared with 2D acquisition, 3D acquisition enables the administration of less radioactivity without loss of image quality. This aspect is especially helpful in research studies on healthy volunteers, in whom the relatively high absorbed dose of ^{18}F prohibits repeated injections. Furthermore, PET/CT scanners from most manufacturers are not equipped with septa, thus dictating 3D scanning. Therefore, it would be advantageous if cardiac PET could be performed in 3D mode without loss of quantitative accuracy.

This study showed a good correlation between K_i determined using 2D and 3D images when blood-sampling input functions were used. In addition, no significant effects of reconstruction method on quantitative results were observed. When blood sampling is used for determination of the input function, 3D acquisition and OSEM reconstruction

are quantitatively as accurate as 2D acquisition and FBP reconstruction, provided the scaling factor in the 3D scatter-correction algorithm is modified to ensure accurate cross-calibration of 2D and 3D acquisitions (*30*).

CONCLUSION

The use of 3D acquisition, combined with blood sampling for determination of the input function, is a good alternative for quantification of cardiac ^{18}F-FDG PET studies. The ascending aorta is the preferred choice for definition of IDIFs for 2D and 3D acquisitions reconstructed with FBP as well as OSEM, resulting in K_i values that show a linear correlation and no bias compared with those obtained using a blood-sampling input function. Iterative reconstruction using attenuation-weighted OSEM is a quantitatively accurate alternative to FBP reconstruction for cardiac ^{18}F-FDG PET. Furthermore, the use of 3D acquisition and OSEM reconstruction may enable less smoothing of the images, leading to a better spatial resolution, which is of importance, for example, in measurements of transmural differences in glucose metabolism. Good correlation and no bias of K_i in relation to K_i values based on FBP images, combined with less image noise, make 3D acquisition with attenuation-weighted OSEM reconstruction the preferred choice for cardiac ^{18}F-FDG PET studies.

ACKNOWLEDGMENTS

REFERENCES

1. Lartizien C, Kinahan PE, Swensson R, et al. Evaluating image reconstruction methods for tumor detection in 3-dimensional whole-body PET oncology imaging. *J Nucl Med.* 2003;44:276–290.
2. Raylman RR, Kison PV, Wahl RL. Capabilities of two- and three-dimensional FDG-PET for detecting small lesions and lymph nodes in the upper torso: a dynamic phantom study. *Eur J Nucl Med.* 1999;26:39–45.
3. Kadrmas DJ, Christian PE, Wollenweber SD, Kohlmyer SG, Stearns CW. Comparative evaluation of 2D and 3D lesion detectability on a full-ring BGO PET scanner [abstract]. *J Nucl Med.* 2002;43(suppl):56P.
4. Hsu CH. A study of lesion contrast recovery for iterative PET image reconstructions versus filtered backprojection using an anthropomorphic thoracic phantom. *Comput Med Imaging Graph.* 2002;26:119–127.
5. Visvikis D, Cheze-LeRest C, Costa DC, et al. Influence of OSEM and segmented attenuation correction in the calculation of standardised uptake values for [^{18}F]FDG PET. *Eur J Nucl Med.* 2001;28:1326–1335.
6. Mesina CT, Boellaard R, Jongbloed G, van der Vaart AW, Lammertsma AA. Experimental evaluation of iterative reconstruction versus filtered back projection for 3D [^{15}O]water PET activation studies using statistical parametric mapping analysis. *Neuroimage.* 2003;19:1170–1179.
7. Boellaard R, van Lingen A, Lammertsma AA. Experimental and clinical evaluation of iterative reconstruction (OSEM) in dynamic PET: quantitative characteristics and effects on kinetic modeling. *J Nucl Med.* 2001;42:808–817.
8. Katoh C, Ruotsalainen U, Laine H, et al. Iterative reconstruction based on median root prior in quantification of myocardial blood flow and oxygen metabolism. *J Nucl Med.* 1999;40:862–867.
9. Bloomfield PM, Myers R, Hume SP, et al. Three-dimensional performance of a small-diameter positron emission tomograph. *Phys Med Biol.* 1997;42:389–400.
10. Dhawan V, Kazumata K, Robeson W, et al. Quantitative brain PET: comparison of 2D and 3D acquisitions on the GE Advance scanner. *Clin Positron Imaging.* 1998;1:135–144.
11. Riddell C, Carson RE, Carrasquillo JA, et al. Noise reduction in oncology FDG PET images by iterative reconstruction: a quantitative assessment. *J Nucl Med.* 2001;42:1316–1323.
12. Sossi V, Oakes TR, Chan GLY, Schulzer M, Ruth TJ. Quantitative comparison of three- and two-dimensional PET with human brain studies. *J Nucl Med.* 1998;39:1714–1719.
13. Sossi V, Oakes TR, Ruth TJ. A phantom study evaluating the quantitative aspect of 3D PET imaging of the brain. *Phys Med Biol.* 1998;43:2615–2630.
14. Lartizien C, Comtat C, Kinahan PE, et al. Optimization of injected dose based on noise equivalent count rates for 2- and 3-dimensional whole-body PET. *J Nucl Med.* 2002;43:1268–1278.
15. Schafers KP, Spinks TJ, Camici PG, et al. Absolute quantification of myocardial blood flow with H$_2$^{15}O and 3-dimensional PET: an experimental validation. *J Nucl Med.* 2002;43:1031–1040.
16. Brink I, Schumacher T, Talazko J, et al. 3D-cardiac-PET: a recommendable clinical alternative to 2D-cardiac-PET? *Clin Positron Imaging.* 1999;2:191–196.
17. Votaw JR, White M. Comparison of 2-dimensional and 3-dimensional cardiac Rb-82 PET studies. *J Nucl Med.* 2001;42:701–706.
18. Watson CC, Newport D, Casey ME, et al. Evaluation of simulation-based scatter correction for 3-D PET cardiac imaging. *IEEE Trans Nucl Sci.* 1997;44:90–97.
19. Ollinger JM. Model-based scatter correction for fully 3D PET. *Phys Med Biol.* 1996;41:153–176.
20. Weinberg IN, Huang SC, Hoffman EJ, et al. Validation of PET-acquired input functions for cardiac studies. *J Nucl Med.* 1988;29:241–247.
21. Choi Y, Hawkins RA, Huang SC, et al. Parametric images of myocardial metabolic-rate of glucose generated from dynamic cardiac PET and 2-[F-18]fluoro-2-deoxy-D-glucose studies. *J Nucl Med.* 1991;32:733–738.
22. Gambhir SS, Schwaiger M, Huang SC, et al. Simple noninvasive quantification method for measuring myocardial glucose-utilization in humans employing positron emission tomography and F-18 deoxyglucose. *J Nucl Med.* 1989;30:359–366.
23. Ohtake T, Kosaka N, Watanabe T, et al. Noninvasive method to obtain input function for measuring tissue glucose-utilization of thoracic and abdominal organs. *J Nucl Med.* 1991;32:1432–1438.
24. van der Weerdt AP, Klein LJ, Boellaard R, et al. Image-derived input functions for determination of MRGlu in cardiac F-18-FDG PET scans. *J Nucl Med.* 2001;42:1622–1629.
25. Hove JD, Iida H, Kofoed KF, et al. Left atrial versus left ventricular input function for quantification of the myocardial blood flow with nitrogen-13 ammonia and positron emission tomography. *Eur J Nucl Med Mol Imaging.* 2004; 31:71–76.
26. Adam LE, Zaers J, Ostertag H, et al. Performance evaluation of the whole-body PET scanner ECAT EXACT HR+ following the IEC standard. *IEEE Trans Nucl Sci.* 1997;44:1172–1179.
27. Brix G, Zaers J, Adam LE, et al. Performance evaluation of a whole-body PET scanner using the NEMA protocol. *J Nucl Med.* 1997;38:1614–1623.
28. Bergström M, Eriksson L, Bohm C, Blomqvist G, Litton J. Correction for scattered radiation in a ring detector positron camera by integral transformation of the projections. *J Comput Assist Tomogr.* 1983;7:42–50.
29. Watson CC. New, faster, image-based scatter correction for 3D PET. *IEEE Trans Nucl Sci.* 2000;47:1587–1594.
30. Boellaard R, van der Weerdt AP, Visser FC, Lammertsma AA. Evaluation of 2D and 3D FDG cardiac PET studies using dynamic scans with alternating 2D and 3D frames [abstract]. *J Nucl Med.* 2003;44(suppl):269P.
31. Defrise M, Kinahan PE, Townsend DW, et al. Exact and approximate rebinning algorithms for 3-D PET data. *IEEE Trans Med Imaging.* 1997;16:145–158.
32. Comtat C, Kinahan PE, Defrise M, Michel C, Townsend DW. Fast reconstruction of 3D PET data with accurate statistical modeling. *IEEE Trans Nucl Sci.* 1998; 45:1083–1089.
33. Boellaard R, Van Lingen A, van Balen SCM, Hoving BG, Lammertsma AA. Characteristics of a new fully programmable blood sampling device for monitoring blood radioactivity during PET. *Eur J Nucl Med.* 2001;28:81–89.
34. Patlak CS, Blasberg RG, Fenstermacher JD. Graphical evaluation of blood-to-brain transfer constants from multiple-time uptake data. *J Cereb Blood Flow Metab.* 1983;3:1–7.
35. Sokoloff L, Reivich M, Kennedy C, et al. The [^{14}C]deoxyglucose method for the measurement of local cerebral glucose utilization: theory, procedure, and normal values in the conscious and anesthetized albino rat. *J Neurochem.* 1977;28:897–916.
36. Huang SC, Phelps ME, Hoffman EJ, et al. Noninvasive determination of local cerebral metabolic rate of glucose in man. *Am J Physiol.* 1980;238:E69–E82.
37. Bland JM, Altman DG. Statistical methods for assessing agreement between two methods of clinical measurement. *Lancet.* 1986;1(8476):307–310.
38. Lubberink M, Schneider H, Bergström M, Lundqvist H. Quantitative imaging and correction for cascade gamma radiation of ^{76}Br with 2D and 3D PET. *Phys Med Biol.* 2002;47:3519–3534.